HHS Public Access

Author manuscript

Nanoscale Horiz. Author manuscript; available in PMC 2020 March 01.

Published in final edited form as:

Nanoscale Horiz. 2019 March 1; 4(2): 426–433. doi:10.1039/C8NH00307F.

Tumour microenvironment-responsive semiconducting polymer-based self-assembly nanotheranostics

Zhen Yang[a,b], **Yunlu Dai**[c], **Lingling Shan**[b], **Zheyu Shen**[b], **Zhantong Wang**[b], **Bryant C. Yung**[b], **Orit Jacobson**[b], **Yijing Liu**[b], **Wei Tang**[b], **Sheng Wang**[b], **Lisen Lin**[b], **Gang Niu**[b], **Pintong Huang**[a], **Xiaoyuan Chen**[b]

[a]Department of Ultrasound in Medicine, the Second Affiliated Hospital of Zhejiang University School of Medicine. No. 88 Jiefang Road, Hangzhou.310009, P. R. China. huangpintong@zju.edu.cn

[b]Laboratory of Molecular Imaging and Nanomedicine (LOMIN), National Institute of Biomedical Imaging and Bioengineering (NIBIB), National Institutes of Health (NIH), Bethesda, Maryland 20892, United States. shawn.chen@nih.gov

[c]Faculty of Health Sciences, University of Macau, Macau SAR 999078, P. R. China. yldai@umac.mo

Abstract

A Pt prodrug polyphenol and gadolinium ion loaded cancer theranostics nanoplatform based on mild acidic pH and thermal sensitive polymer was designed for photoacoustic (PA)/ magnetic resonance(MR)/ positron emission tomography (PET) multimodal imaging-guided chemo-photothermal combination therapy. The Pt drug release can be controlled by tumour-specific acidic pH and heat generated by external NIR irradiation. The nanoparticles were stable under normal physiological environment and released the drug under tumour acidic pH and NIR laser irradiation, which can reduce the side effect of drug to normal organs. Moreover, the MR signal can be significantly enhanced (~3-fold increase in T1 relaxivity) under the acidic tumour microenvironment, which is favorable for cancer diagnosis. The nanoparticles exhibited excellent tumour accumulation and led to complete tumour eradication with low power NIR laser irradiation. This promising approach provides a new avenue for imaging-guided combination therapy.

Graphical Abstract

The nanoparticles exhibited excellent tumor accumulation and led to complete tumor eradication with low power NIR laser irradiation.

Electronic Supplementary Information (ESI) available: See DOI: 10.1039/c8nh00307f

Conflicts of interest

The authors declare no competing financial interest.

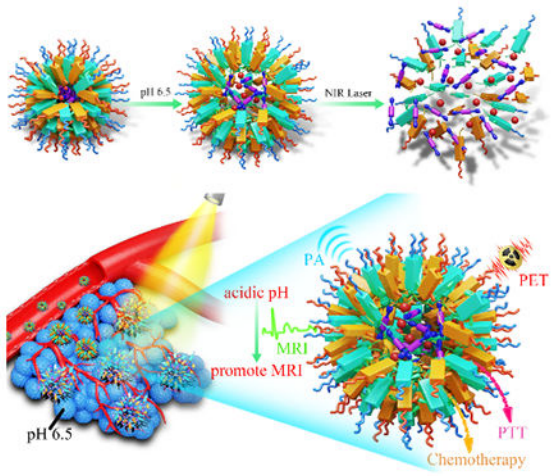

1. Introduction

Early diagnosis of cancer is essential for cancer management and is accomplished through highly sensitive, quantitative detection, which can promote the chance for cure and saving patients' lives. Multimodal imaging can improve the efficiency of current cancer diagnostic methods by exploiting the strengths of multiple imaging techniques.[1–5] Currently, positron emission tomography (PET), as a specialized radiologic procedure, has been widely used in the clinic demonstrating high sensitivity, resolution, and quantitative ability.[6, 7] Magnetic resonance imaging (MRI) is another robust noninvasive technique for visualizing soft-tissue structures with greater spatial resolution.[8, 9] Nowadays, Gd^{3+} based chelates are the most popular contrast agents for T_1-weighted MRI thanks to the presence seven unpaired electrons with parallel spin.[10, 11] To date, photoacoustic (PA) imaging has been employed as a prominent imaging modality by integrating optical and ultrasonic waves with deep tissue penetration and high spatial resolution.[12, 13] There are various optical contrast agents with absorption in the NIR region for PA imaging.[14, 15]

A large number of chemotherapeutics have been employed for cancer therapy. However, there are still many inevitable issues, such as multidrug resistance and side effects to normal organs.[16–18] To enhance cancer treatment efficacy, combination chemotherapy with various therapies has attracted a great deal of attentions to achieve synergistic therapeutic effect.[19] Photothermal therapy (PTT) is an important method that exploits optically active agents to convert the light energy into heat by laser irradiation for tumour ablation.[20–22] Therefore, the combination of PTT and chemotherapy is a promising method to improve cancer therapy efficacy.[23, 24]

A number of nanomaterials have been demonstrated to improve cancer therapy and reduce side effects to normal organs.[25, 26] Semiconducting organic molecule based nanomaterials have been employed as promising carriers for biomedical applications owing to numerous advantages over other nanomaterials.[27–29] Perylene diimide (PDI) has attracted great interest as a scaffold material for encapsulation or covalent conjugation of therapeutic agents, aiming to achieve robust stability, excellent photothermal efficiency, and good biocompatibility for

cancer theranostics.[30, 31] In addition, the coordination chemistry between metal and polyphenols has been exploited for various biomedical applications.[32, 33] Recently, we reported on the synthesis of the platinum (Pt) prodrug polyphenols for reactive oxygen species enhanced chemotherapy.[34, 35]

Herein, we have constructed a Pt prodrug polyphenols and gadolinium ion (Gd^{3+}) loaded cancer theranostics nanoplatform based on pH and thermal sensitive polymer with MRI promoted property for multimodal imaging-guided chemo-photothermal combination therapy. pH/thermal sensitive block copolymer poly(ethylene glycol)-perylene diimide-poly(diisopropanol amino ethyl methacrylate) (PEG-PDI-PDPA, termed as PDDA) and 2-Octyldodecyl-perylene diimide-poly(ethylene glycol) (PEG-PDI-C_{20}), termed as PDC) were synthesized. PDPA is a promising polymer to design tumour microenvironment acid-sensitive system.[36–38] Moreover, PDC could improve the hydrophobic ability of the nanoparticles, which may reduce drug leakage in the physiological environment. As the next generation semiconducting material, PDI can be applied for PA imaging and photothermal therapy because of the strong NIR absorption. Due to the strong coordination between the metal ion and phenolic ligands, the Gd^{3+} is able to coordinate with the polyphenols of the prodrug to achieve Gd-Pt prodrug complexes. Moreover, the PDPA can also interact with polyphenols by electrostatic interactions when the pH is lower than 6.5. Then, the PDDA and PDC can encapsulate the Gd-Pt prodrug complexes to form the Gd/Pt prodrug PDPA/PDC nanoparticles (GPDPA NPs) theranostics nanoplatform after the pH is adjusted to 8.0 (Scheme 1). As the Gd^{3+} was in the hydrophobic core of the nanoparticles, the MR signal was reduced due to the low exchange of water molecules surrounding Gd^{3+} complexes. Subsequently, MR signal could be promoted to monitor the Pt drug release when the GPDPA NPs were accumulated in the tumour under mild acidic pH. The integration of chemotherapy and PTT by the GPDPA NPs exhibited a synergistic effect and promoted treatment efficacy.

2. RESULTS AND DISCUSSION

2.1 Controlled synthesis and characterization of GPDPA NPs.

PEG-PDI-PDPA polymer was synthesized by atom-transfer radical polymerization (ATRP), and synthesis routes and characterizations of PEG-PDI-PDPA were given in Scheme 2 and Fig. S1-S11, respectively. The PEG-PDI-C_{20} was obtained by our previous protocols.[39] Pt prodrug polyphenol was prepared by our previous protocol and characterized by FTIR, ^1H NMR spectrum and mass spectrometry (Fig. S11-S13).[32] Due to the strong coordination between polyphenols and metal, the Gd^{3+} was employed to chelate with Pt prodrug polyphenols.[40] The PDI based polymers could encapsulate the Pt prodrug polyphenols and Gd^{3+} in the core to form stable GPDPA NPs with high prodrug loading efficiency (20 %), and Gd^{3+} occupied 3 % of the nanoparticles for MRI by ICP-OES (Table S1 and Fig. S14). As given by the transmission electron microscopy (TEM) image in Fig. 1a, the monodisperse GPDPA NPs were prepared with a diameter ≈50 nm. Dynamic light scattering (DLS) was used to measure the average hydrodynamic size of the GPDPA NPs (Fig. S15). The average hydrodynamic size of 55 ± 7 nm by DLS matched well with the TEM observation. When the pH decreased to 6.5 (acidic tumour microenvironment), the GPDPA

NPs swelled up to 81 ± 13 nm due to the PDPA protonation (Fig. 1b and Fig. S16). The DLS and TEM images of GPDPA NPs under pH 6.5 and 671 nm laser irradiation were also given in Fig. S15 and Fig. 1c. There were only NPs aggregates remaining when the GPDPA NPs were irradiated with 671 nm laser (0.3 W/cm^2, 5 min) under pH 6.5 mild acidic environment owing to the great photothermal effect of PDI and the PDPA protonation in the GPDPA NPs. The UV-vis spectrum of GPDPA NPs and Gd-Pt polyphenols complexes were displayed in Fig. S17, where the strong absorption peak at 671 nm of GPDPA NPs can be attributed to the H-aggregate and monomer bands of PDI in the GPDPA NPs, which was beneficial for photothermal applications.[39] Photothermal conversion capacity was further investigated by 671 nm NIR laser irradiation under various GPDPA NPs concentrations and laser powers. The temperature and photothermal images of GPDPA NPs solution were determined by an infrared thermal camera. First, the laser power was kept at 0.5 W/cm^2 and the GPDPA NPs were irradiated with a 671 nm laser under various GPDPA NPs concentrations (0, 0.2, 1.0, 2.5, 5.0 mg/mL) for 5 min. As the concentration increased from 0 to 5.0 mg/mL, the temperature increased from ~24.0 °C to 51.5, 64.2, 71.6, and 79.5 °C (Fig. 1d). Then, the GPDPA NPs concentrations were kept at 5 mg/mL, and the laser power increased from 0.1 to 1.0 W/cm^2 (Fig. 1e). The temperature increased from ~24.0 °C to 25.3, 34.2, 52.6, 66.1, 71.0, 76.0 °C after 5 min irradiation. In contrast, the negligible temperature rise can be found for the pure water. All the above results indicated that the GPDPA NPs were excellent candidates converting NIR energy to heat efficiently, which can be employed for photothermally triggered release.

Since the Pt prodrug polyphenols were encapsulated in the core of the GPDPA NPs, the NIR and pH triggered Pt drug release behaviors of the GPDPA NPs were further investigated under different conditions (Fig. 1f). GPDPA NPs were dispersed in PBS titrated to two kinds of pH values (7.4 and 6.5) with laser irradiation at 671 nm for 10 min at each time timepoint. The supernatants were then collected and analyzed for Pt by ICP-OES. The release percentage of Pt reached up to 81 % within 24 h at pH 6.5 by laser irradiation. In contrast, at pH 7.4, only 21 % of Pt released under laser irradiation. This can be attributed to the low pH leading to the protonation of PDPA and the expansion of GPDPA NPs, thus enabling the release of Pt drugs by the photothermal effect of PDI. The GPDPA NPs also demonstrated high stability with negligible drug release at pH 7.4 without laser irradiation. GPDPA NPs can release the drugs in mild acidic tumour environment by laser irradiation. We further investigated the drug leakage in the fetal bovine serum (FBS), only 10% of Pt drug was released within 24 h (Fig. S18), which indicated that the GPDPA NPs could prevent drug leakage in the blood and reduce the side effect of the anti-cancer drug to normal tissues.

Owing to the strong absorption of PDI in the NIR region, the PA/ultrasound (US) performance GPDPA NPs *in vitro* was investigated. As given in Fig. 1g, the PA intensity of GPDPA NPs linearly correlated with the concentration of GPDPA NPs. Therefore, the GPDPA NPs were excellent candidates to enhance PA imaging *in vivo*. Moreover, the *in vitro* MR imaging contrast performance of GPDPA NPs was further explored. Longitudinal proton relaxation times (T_1) of GPDPA NPs under two different pH (7.4 and 6.5) and commercial Gd^{3+}-based MR contrast agent Magnevist (gadopentetate dimeglumine) were displayed in Fig. 1h. The T_1-weighted MR images of GPDPA NPs and Magnevist with various Gd concentrations were also displayed in Fig. S19. All the MR intensities exhibited

a dose-dependent brightening effect. And the T_1 relaxivity of GPDPA NPs at pH 7.4 was 3.547 mM^{-1} s^{-1}, which was similar to the 4.351 mM^{-1} s^{-1} of Magnevist. Interestingly, about 3-fold enhancement of T_1 relaxivity (10.27 mM^{-1} s^{-1}) was obtained when the pH of GPDPA NPs was 6.5 (Table S2), because the low pH led to the protonation of PDPA, and water can penetrate into the core of GPDPA NPs, resulting in swelling. Consequently, the exchange between bulk and bound water coordinating Gd complex was affected and enhanced the T_1 relaxivity.[41] In addition, strong hydrogen bonds between water and polyphenols at low pH can also enhance the T_1 relaxivity.[42] Therefore, the MR imaging can be used to monitor the tumour mildly acidic tumour pH.

2.2 *In vitro* cell effect with GPDPA NPs.

The cell cytotoxicity of GPDPA NPs with different Pt concentrations under 671 nm laser irritation for 5 min with a power of 0.3 W/cm^2 was tested by a MTT assay (Fig. 2a). As given in Table S3, compared with the GPDPA NPs without laser irritation (half-maximal inhibitory concentration, IC_{50} = 1.865 μM) and cisplatin (IC_{50} = 0.634 μM), the GPDPA NPs showed obviously high cytotoxicity to U87MG cells (IC_{50} = 0.316 μM). The laser irritation not only triggered the Pt drug release, but also led to phototoxicity with high concentration of GPDPA NPs. Meanwhile, the low toxicity of GPDPA NPs without laser irritation can reduce the side effect of the Pt drugs to normal organs. Subsequently, the cell association of GPDPA NPs was further investigated by measuring the Gd content in the cells by ICP-OES (Fig. 2b). The nanoparticles were incubated with U87MG cells for 2, 8, and 24 h. Moreover, longer incubation times led to higher cell internalization of GPDPA NPs. Furthermore, the cell viabilities following GPDPA NPs treatment under various conditions were visualized by the live/dead staining viability/cytotoxicity kit. The live and dead cells were stained by green-fluorescent calcein-AM and red-fluorescent ethidium homodimer-1 (EthD-1), respectively. Negligible red signals were observed in the control and laser groups (Fig. 2c). There was no measurable phototoxicity of the laser irradiation without GPDPA NPs. Most of the cells showed green fluorescence from the GPDPA NPs group without laser irritation, and only a fraction of the cells displayed red signals due to the minor release of Pt drugs released from GPDPA NPs. In contrast, a much higher level of red fluorescence can be observed after being exposed to 671 nm laser with a power of 0.1 W/cm^2 for 3 min. This could be attributed to the photothermally triggered drug release, which led to cell apoptosis. All cells were killed by prolonging the irradiation time to 5 min thanks to the chemo-photothermal combination therapy.

2.3. Both *in vitro* and *in vivo* multi-modal imaging with the GPDPA NPs

In vivo multimodal imaging capacity of GPDPA NPs was further studied to investigate the tumour diagnosis and accumulation abilities of GPDPA NPs. Thanks to the strong absorption of GPDPA NPs in the NIR region, PA imaging capability of GPDPA NPs was studied first by administrating GPDPA NPs intravenously and the PA/US signals in a tumour were recorded and quantified with the laser excitation at 671 nm at various time points. As given in Fig. 3a and b, the PA signal intensity increased gradually over time and plateaued at 24 h post-injection, and the administration of GPDPA NPs caused almost four-fold promotion of PA signal intensity, indicating the promise of GPDPA NPs for PA imaging-guided cancer therapy.

As the Gd^{3+} ions were encapsulated and chelated with polyphenols in the GPDPA NPs, we evaluated the T_1-weighted MR imaging property of GPDPA NPs *in vivo*. GPDPA NPs were injected to the U87MG xenograft tumour model by tail vein. Compared with the pre-injection, the T_1 contrast reached its highest signal at 24 h post-injection (Fig. 3c and S20). The quantitative analysis of tumour signal was further evaluated by using ΔSNR from the equations S1 and S2.[43] As shown in Fig. 3d, the ΔSNR was as high as 127 ± 10% at 24 h post-injection, which should be attributed to excellent tumour accumulation of GPDPA NPs and MR signal enhancement of GPDPA NPs in acidic tumour microenvironment by the protonation of PDPA. These results suggest that the GPDPA NPs can be utilized as excellent T_1-weighted MRI contrast agent for monitoring the acidic tumour microenvironment.

PET is a highly sensitive clinical imaging technique, which plays an essential role in cancer diagnosis. In this study, the long half-life of ^{64}Cu was employed for GPDPA NPs labelling *via* efficient chelating thiol groups on the surface of GPDPA NPs.[44] The whole-body PET images and quantitative biodistribution at various time points were displayed in Fig. 3e and 3f. The GPDPA NPs could accumulate in the tumour at 1 h post-injection. The strongest PET signal of GPDPA NPs in the tumour can be observed at 24 h post-injection with tumour uptake of about 6 % ID/g. Then, the tumour uptake decreased slightly after 24 h. Furthermore, the gamma-counting of major organs were presented at 48 h post-injection (Fig. 3g), which matched with the PET results. The above PET results further confirmed effective tumour accumulation of GPDPA NPs and reached a plateau at 24 h post-injection, which was consistent with the PA and MR imaging results. The *in vivo* PA/MR/PET multimodal imaging indicates the excellent performance of GPDPA NPs for cancer diagnosis and high tumour accumulation guiding the efficient synergistic chemo-photothermal combination therapy.

2.4 *In vivo* photothermal property and cancer therapy with GPDPA NPs.

Based on the excellent photothermal conversion efficiency *in vitro*, we evaluated the photothermal effect in U87MG xenograft tumour mice model. Because the tumour accumulation of GPDPA NPs reached a maximum at 24 h post-injection as confirmed by PA/MR/PET multimodal imaging, the tumour sites were shined by a 671 nm NIR laser with two different powers (0.5 and 0.3 W/cm^2). In addition, PBS was administered intravenously to mice with NIR laser irradiation at 24 h post-injection as a control group. The temperature of the mice was monitored by an infrared thermal camera. As given in Fig. 4a and S21, the tumour temperature of mice administered with PBS were increased to 36 °C by a power of 0.5 W/cm^2 for 10 min. However, the tumour temperature of mice treated with GPDPA NPs was increased up to 39 and 48 °C by the power settings of 0.3 and 0.5 W/cm^2, respectively. The above results confirmed the excellent photothermal conversion property of GPDPA NPs in an animal model. Furthermore, the therapeutic capability of GPDPA NPs was conducted *in vivo* (Fig. 4b and S22). U87MG xenograft tumour mice were randomized to six groups: PBS, GPDPA NPs + 0.5 W/cm^2 laser, GPDPA NPs + 0.3 W/cm^2 laser, GPDPA NPs, free cisplatin, and PBS + 0.5 W/cm^2 laser. All the groups received a single treatment. The 0.5 W/cm^2 laser irradiation did not inhibit tumour growth, suggesting the safety of laser irradiation and no overheating without GPDPA NPs injection. The mice administered with GPDPA NPs or free cisplatin did not experience complete tumour regression, whereas the

mice treated with the GPDPA NPs + 0.3 W/cm^2 laser and GPDPA NPs + 0.5 W/cm^2 laser showed pronounced tumour inhibition with a greatly prolonged survival time (Fig. 4c). Interestingly, the tumours from the GPDPA NPs + 0.5 W/cm^2 group were completely absent, presumably because of the tumour acidic pH/photo-triggered Pt drug release and photothermal synergistic combination therapy. In contrast, the 0.3 W/cm^2 laser may only improve the Pt drugs release from GPDPA NPs at the tumour site. Compared with the PBS or laser irradiation group, significant tumour apoptosis and necrosis were found from GPDPA NPs treatment groups by hematoxylin and eosin (H&E) staining of the tumour section after 48 h post-administration (Fig. 4e), indicating the improved synergistic chemo-photothermal combination therapy. The terminal deoxynucleotidyl transferase dUTP nick end labelling (TUNEL) assay was further used to investigate the DNA damage of tumour section at 48 h post-administration. Obviously, most tumour cells underwent apoptosis by GPDPA NPs with laser irradiation treatments (Fig. S23), suggesting the contribution of Pt drugs release from the GPDPA NPs. In addition, there was no significant body weight loss from all the groups during the whole treatment thanks to the negligible side effects of the therapy (Fig. 4d). No obvious pathological abnormalities and inflammation were found in major organs of mice after the whole therapy (Fig. S24), which suggest the great biocompatibility of GPDPA NPs.

3. Conclusions

In this work, we developed a new nanoplatform integrating PA/MR/PET multimodal imaging and photothermal promoted cancer chemotherapy based on encapsulating Pt prodrug polyphenols and Gd^{3+} by mildly acidic pH sensitive PDI/PDPA polymer. Two kinds of polymers, PEG-PDI-PDPA and PEG-PDI-C_{20} were synthesized and self-assembled to form GPDPA NPs, which were responsive to mildly acidic pH/NIR laser for anticancer drug release. The GPDPA NPs showed effective photothermal conversion to trigger drug release and kill tumour cells under 671 nm laser irradiation as well. Interestingly, the MR signal could be significantly enhanced (~3-fold increase in T_1 relaxivity) under the acidic tumour microenvironment, which was beneficial to monitor the pH variation and drug release. The *in vivo* PA/MR/PET multimodal imaging indicated extremely high tumour accumulation of GPDPA NPs *via* the EPR effect, which can be utilized to guide cancer treatment. The administration of GPDPA NPs effectively inhibited tumour growth with NIR laser irradiation, achieving the synergistic effect for chemo-photothermal combination therapy. We expect that this study may establish a novel paradigm for engineering nanoparticle responses to the tumour microenvironment for improving cancer theranostics in the clinic.

Supplementary Material

Refer to Web version on PubMed Central for supplementary material.

Acknowledgements

This study was supported by National Natural Science Foundation of China (No. 81527803, 81420108018), the Intramural Research Program (IRP) of the National Institute of Biomedical Imaging and Bioengineering (NIBIB), National Institutes of Health (NIH), the intramural research program of Faculty of Health Sciences, University of Macau, and the Start-up Research Grant (SRG) of University of Macau (SRG2018-00130-FHS).

Notes and references

1. Kim J, Piao Y and Hyeon T, Chem. Soc. Rev, 2009, 38, 372–390. [PubMed: 19169455]
2. Weissleder R, Nahrendorf M and Pittet MJ, Nat. Mater, 2014, 13, 125. [PubMed: 24452356]
3. de Jong M, Essers J and van Weerden WM, Nat. Rev. Cancer, 2014, 14, 481. [PubMed: 24943811]
4. Bardhan R, Lal S, Joshi A and Halas NJ, Acc. Chem. Res, 2011, 44, 936–946. [PubMed: 21612199]
5. Li JJ, Cheng FF, Huang HP, Li LL and Zhu JJ, Chem. Soc. Rev, 2015, 44, 7855–7880. [PubMed: 26214317]
6. Sun X, Cai W and Chen X, Acc. Chem. Res, 2015, 48, 286–294. [PubMed: 25635467]
7. Goel S, England CG, Chen F and Cai W, Adv. Drug Del. Rev, 2017, 113, 157–176.
8. Ahrens ET and Bulte JWM, Nat. Rev. Immunol, 2013, 13, 755. [PubMed: 24013185]
9. Guo J, Yang WL and Wang CC, Adv. Mater, 2013, 25, 5196–5214. [PubMed: 23996652]
10. Verwilst P, Park S, Yoon B and Kim JS, Chem. Soc. Rev, 2015, 44, 1791–1806. [PubMed: 25622561]
11. Bennett KM, Jo J, Cabral H, Bakalova R and Aoki I, Adv. Drug Del. Rev, 2014, 74, 75–94.
12. Kim C, Favazza C and Wang LHV, Chem. Rev, 2010, 110, 2756–2782. [PubMed: 20210338]
13. Nie LM and Chen XY, Chem. Soc. Rev, 2014, 43, 7132–7170. [PubMed: 24967718]
14. Weber J, Beard PC and Bohndiek SE, Nat. Methods, 2016, 13, 639–650. [PubMed: 27467727]
15. Jiang YY and Pu KY, Small, 2017, 13, 1700710.
16. Iyer AK, Singh A, Ganta S and Amiji MM, Adv. Drug Del. Rev, 2013, 65, 1784–1802.
17. Holohan C, Van Schaeybroeck S, Longley DB and Johnston PG, Nat. Rev. Cancer, 2013, 13, 714–726. [PubMed: 24060863]
18. Bouwman P and Jonkers J, Nat. Rev. Cancer, 2012, 12, 587. [PubMed: 22918414]
19. Fan W, Yung B, Huang P and Chen X, Chem. Rev, 2017, 117, 13566–13638. [PubMed: 29048884]
20. Chen QW, Wen J, Li HJ, Xu YQ, Liu FY and Sun SG, Biomaterials, 2016, 106, 144–166. [PubMed: 27561885]
21. Zou LL, Wang H, He B, Zeng LJ, Tan T, Cao HQ, He XY, Zhang ZW, Guo SR and Li YP, Theranostics, 2016, 6, 762–772. [PubMed: 27162548]
22. Nam J, Son S, Ochyl LJ, Kuai R, Schwendeman A and Moon JJ, Nat. Commun, 2018, 9, 1074. [PubMed: 29540781]
23. Luo DD, Carter KA, Miranda D and Lovell JF, Adv. Sci, 2017, 4, 1600106.
24. Yun SH and Kwok SJJ, Nature Biomedical Engineering, 2017, 1, 16.
25. Lin H, Wang XG, Yu LD, Chen Y and Shi JL, Nano Lett, 2017, 17, 384–391. [PubMed: 28026960]
26. Dai YL, Xiao HH, Liu JH, Yuan QH, Ma PA, Yang DM, Li CX, Cheng ZY, Hou ZY, Yang PP and Lin J, J. Am. Chem. Soc, 2013, 135, 18920–18929. [PubMed: 24279316]
27. Zhou L, Lv F, Liu L, Shen G, Yan X, Bazan GC and Wang S, Adv. Mater, 2018, 30, 1704888.
28. Fateminia SMA, Mao Z, Xu S, Yang Z, Chi Z and Liu B, Angew. Chem. Int. Ed, 2017, 56, 12160–12164.
29. Lyu Y, Zeng J, Jiang Y, Zhen X, Wang T, Qiu S, Lou X, Gao M and Pu K, ACS Nano, 2018, 12, 1801–1810. [PubMed: 29385336]
30. Tang W, Yang Z, Wang S, Wang Z, Song J, Yu G, Fan W, Dai Y, Wang J, Shan L, Niu G, Fan Q and Chen X, ACS Nano, 2018, 12, 2610–2622. [PubMed: 29451774]
31. Hu X, Lu F, Chen L, Tang Y, Hu W, Lu X, Ji Y, Yang Z, Zhang W, Yin C, Huang W and Fan Q, ACS Appl. Mater. Interfaces, 2017, 9, 30458–30469. [PubMed: 28825456]
32. Dai Y, Guo J, Wang T-Y, Ju Y, Mitchell AJ, Bonnard T, Cui J, Richardson JJ, Hagemeyer CE, Alt K and Caruso F, Adv. Healthcare Mater, 2017, 6, 1700467.
33. He C, Liu D and Lin W, Chem. Rev, 2015, 115, 11079–11108. [PubMed: 26312730]
34. Dai Y, Cheng S, Wang Z, Zhang R, Yang Z, Wang J, Yung BC, Wang Z, Jacobson O, Xu C, Ni Q, Yu G, Zhou Z and Chen X, ACS Nano, 2018, 12, 455–463. [PubMed: 29293312]
35. Dai Y, Yang Z, Cheng S, Wang Z, Zhang R, Zhu G, Wang Z, Yung BC, Tian R, Jacobson O, Xu C, Ni Q, Song J, Sun X, Niu G and Chen X, Adv. Mater, 2018, 30, 1704877.

36. Wang Y, Zhou K, Huang G, Hensley C, Huang X, Ma X, Zhao T, Sumer BD, DeBerardinis RJ and Gao J, Nat. Mater, 2013, 13, 204. [PubMed: 24317187]
37. Wang D, Wang T, Liu J, Yu H, Jiao S, Feng B, Zhou F, Fu Y, Yin Q, Zhang P, Zhang Z, Zhou Z and Li Y, Nano Lett, 2016, 16, 5503–5513. [PubMed: 27525587]
38. Dai Y, Xu C, Sun X and Chen X, Chem. Soc. Rev, 2017, 46, 3830–3852. [PubMed: 28516983]
39. Yang Z, Tian R, Wu J, Fan Q, Yung BC, Niu G, Jacobson O, Wang Z, Liu G, Yu G, Huang W, Song J and Chen X, ACS Nano, 2017, 11, 4247–4255. [PubMed: 28345873]
40. Guo J, Ping Y, Ejima H, Alt K, Meissner M, Richardson JJ, Yan Y, Peter K, Elverfeldt D. v., Hagemeyer CE and Caruso F, Angew. Chem. Int. Ed, 2014, 53, 5546–5551.
41. Hu X, Liu G, Li Y, Wang X and Liu S, J. Am. Chem. Soc, 2015, 137, 362–368. [PubMed: 25495130]
42. Fan J-X, Zheng D-W, Mei W-W, Chen S, Chen S-Y, Cheng S-X and Zhang X-Z, Small, 2017, 13, 1702714.
43. Shen Z, Chen T, Ma X, Ren W, Zhou Z, Zhu G, Zhang A, Liu Y, Song J, Li Z, Ruan H, Fan W, Lin L, Munasinghe J, Chen X and Wu A, ACS Nano, 2017, 11, 10992–11004. [PubMed: 29039917]
44. Lu N, Fan W, Yi X, Wang S, Wang Z, Tian R, Jacobson O, Liu Y, Yung BC, Zhang G, Teng Z, Yang K, Zhang M, Niu G, Lu G and Chen X, ACS Nano, 2018, 12, 1580–1591. [PubMed: 29384652]

Conceptual insights

Engineering the next generation of nanoplatforms to enhance theranostic performance and reduce side effect of anticancer agents to normal organs remains a persistent challenge for nanomedicine. Organic semiconducting materials have emerged as a promising platform for novel nanomedicines development due to the excellent photothermal conversion efficiency and good biocompatibility. The photothermal property of the nanoparticles is exploited to trigger drug release and promote chemo-photothermal combination therapy, permitting specific cancerous cell treatment with a low drug dose and resulting in complete tumour eradication with nanoparticles administration under 671 nm laser irradiation. We believe that the designed nanoparticles can be regarded as an efficient nanomedicine platform for both multimodal imaging and cancer therapy.

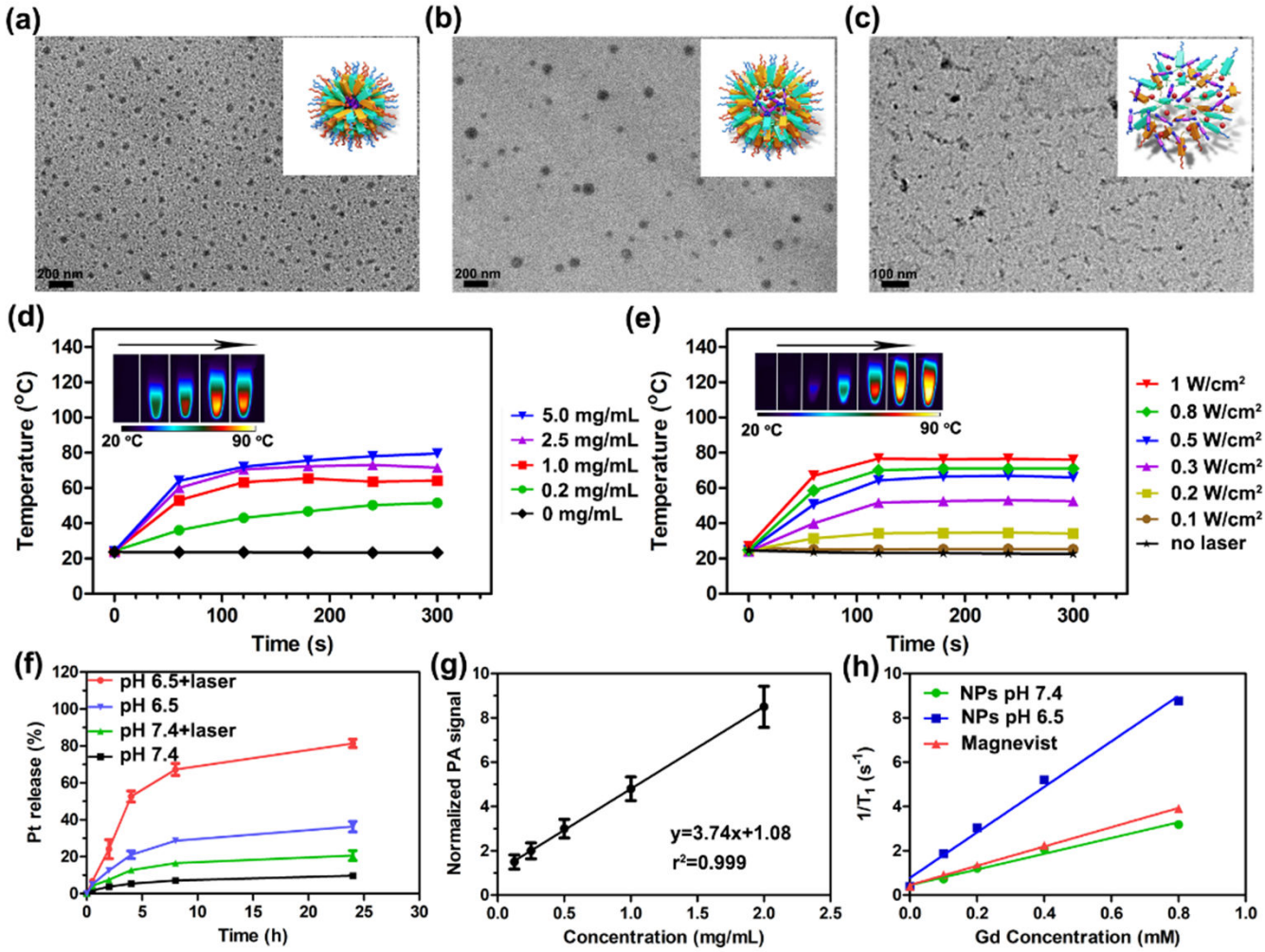

Fig. 1.

The TEM images of GPDPA NPs at pH 7.4 (a), pH 6.5 (b) and pH 6.5 with NIR laser irradiation at a power of 0.5 W/cm^2 for 5 min (c). The size of GPDPA NPs increased from 54.5 ± 7.1 nm to 80.8 ± 13.3 nm by DLS due to the PDPA protonation. There were only aggregates remaining owing to the great photothermal effect of PDI and the PDPA protonation in the GPDPA NPs. The temperature variation of various GPDPA NPs concentrations by a 0.5 W/cm^2 laser irradiation for 5 min with photothermal heating images (d). The temperature variation of various laser powers with fixed GPDPA NPs concentration (5 mg/mL) in aqueous solution (e). The GPDPA NPs exhibited excellent photothermal conversion property, which is favorable for further *in vivo* PA imaging and chemo-photothermal combination therapy. The release of Pt from GPDPA NPs with various conditions with pH/NIR light-sensitive release (f). The PA signals of GPDPA NPs as a function of concentration with 680 nm laser irradiation (g). Longitudinal relaxation rates ($1/T_1$) of GPDPA NPs at pH 7.4 and 6.5, and Magnevist as a function of Gd concentration (h). The T_1 relaxivity (r_1 value) of GPDPA NPs at pH 6.5 was 10.27 mM^{-1} s^{-1}, about a 3-fold enhancement of that at pH 7.4 (3.547 mM^{-1} s^{-1}). The r_1 value of Magnevist was only

4.351 mM^{-1} s^{-1}. The r_1 value of GPDPA NPs could be promoted under acidic pH. Error bars (f and g), s.d. (n=3 replicates).

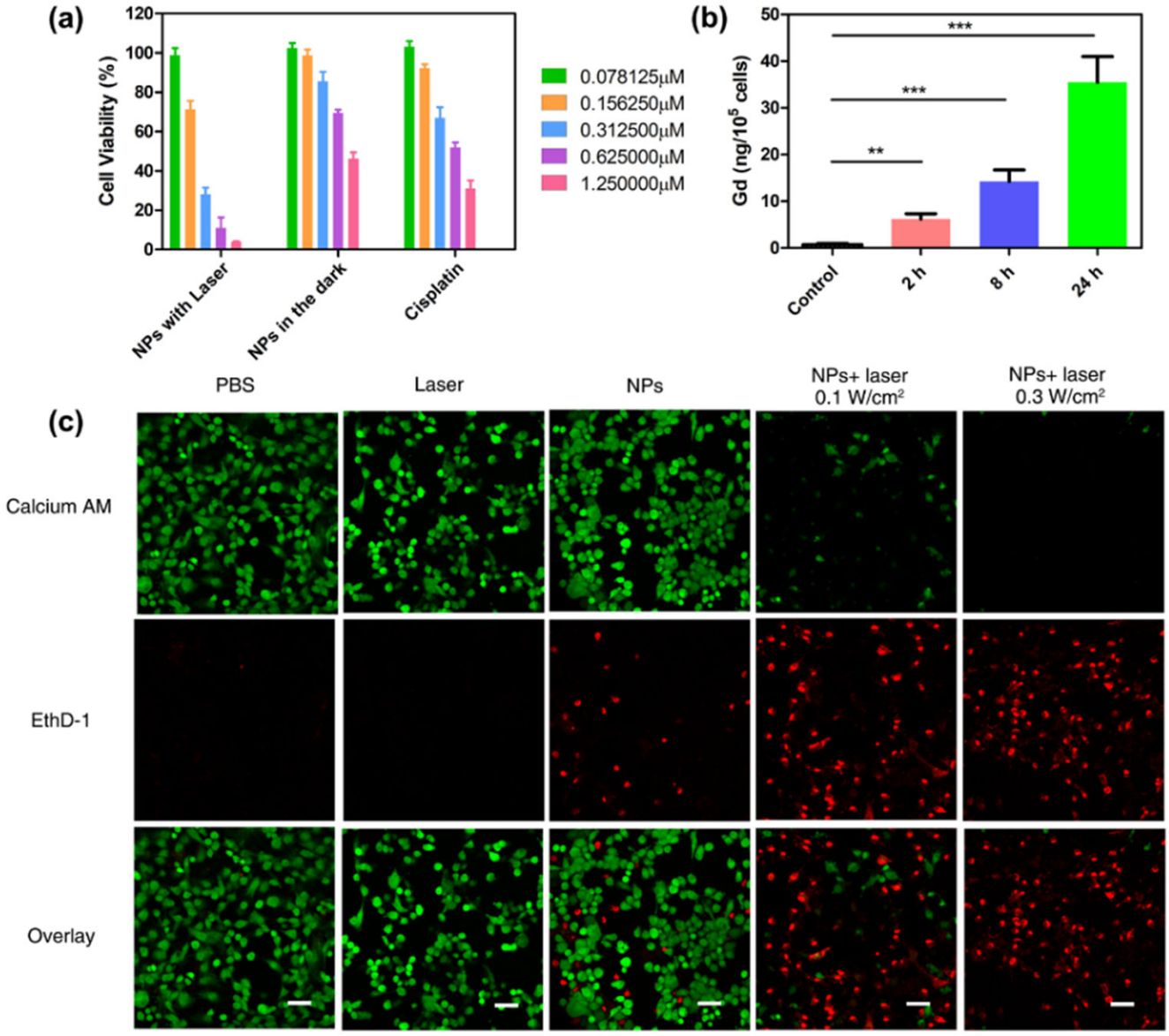

Fig. 2.

Cell viability and cell association study. (a) The cell viability of U87MG cells treated by cisplatin, GPDPA NPs without and GPDPA NPs with laser irradiation at a power of 0.3 W/cm^2 for 10 min under various Pt concentrations for 48 h. The IC_{50} of GPDPA NPs with laser irradiation was 0.316 μM, which was much lower than the GPDPA NPs in the dark (IC_{50} = 1.865 μM) due to the photothermally triggered drug release and photothermal destruction of the cells (Values are mean ± s.d., n=4). (b) Mass of Gd internalized in U87MG cells after incubation with GPDPA NPs for various time points. (*P* values, $^{**}P < 0.01$, $^{***}P < 0.001$, are calculated by *t*-test.). (c) Confocal microscopy images of U87MG cells treated with various formulations and stained by live and dead cells assays. The live and dead cells were stained by Calcium AM (green fluorescence) and EthD-1 (red fluorescence), respectively. There were ignorable live cells remaining after treatment with

GPDPA NPs and 0.3 W/cm^2 laser irradiation, whereas a high level of green fluorescence can be observed in the GPDPA NPs group without laser irritation, indicating the excellent photothermal conversion property of GPDPA NPs. Scale bar: 50 μm.

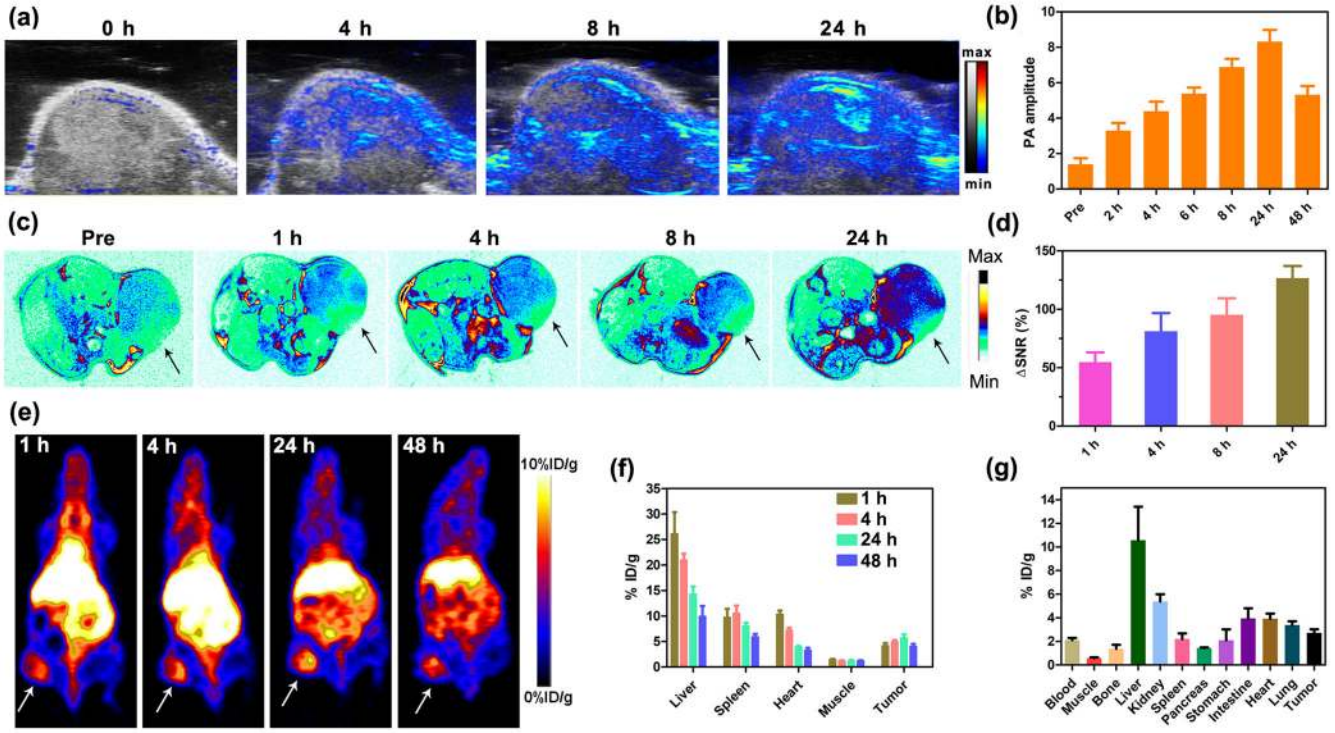

Fig. 3.

In vivo multimodal imaging. (a) *In vivo* PA/US images of xenograft U87MG tumour-bearing mice at tumour section after various post-injection time points and (b) quantitative analysis of the PA signal intensity. The PA amplitude was as high as 8.32 ± 0.66 at 24 h post-injection (c) *In vivo* T_1-weighted MR images of U87MG tumour-bearing mice after 1, 4, 8, and 24 h after intravenous injection of GPDPA NPs and quantitative analysis of tumour by Δ SNR calculation (d). The whole-body PET images of the U87MG tumour-bearing mice (e), the arrows indicate the tumour location. The tumour accumulation reached to 6 %ID/g at 24 h post-injection and the bio-distribution of GPDPA NPs in major organs and tumour by ROI at various post-injection time points (f). The biodistribution of GPDPA NPs in most organs at 72 h post-injection by gamma counter (g). The *in vivo* multimodal imaging suggested the high tumour accumulation of GPDPA NPs at the tumour site, which could be exploit for further chemo-photothermal combination therapy. More importantly, the MR signal was much stronger compared with the PA and PET signals at 24 h post-injection. This can be attributed to the acidic pH in tumour which could protonate PDPA and more, water can penetrate into the core of GPDPA NPs to promote MR signal. Error bars (b, d, f and g), s.d. (n=3 replicates).

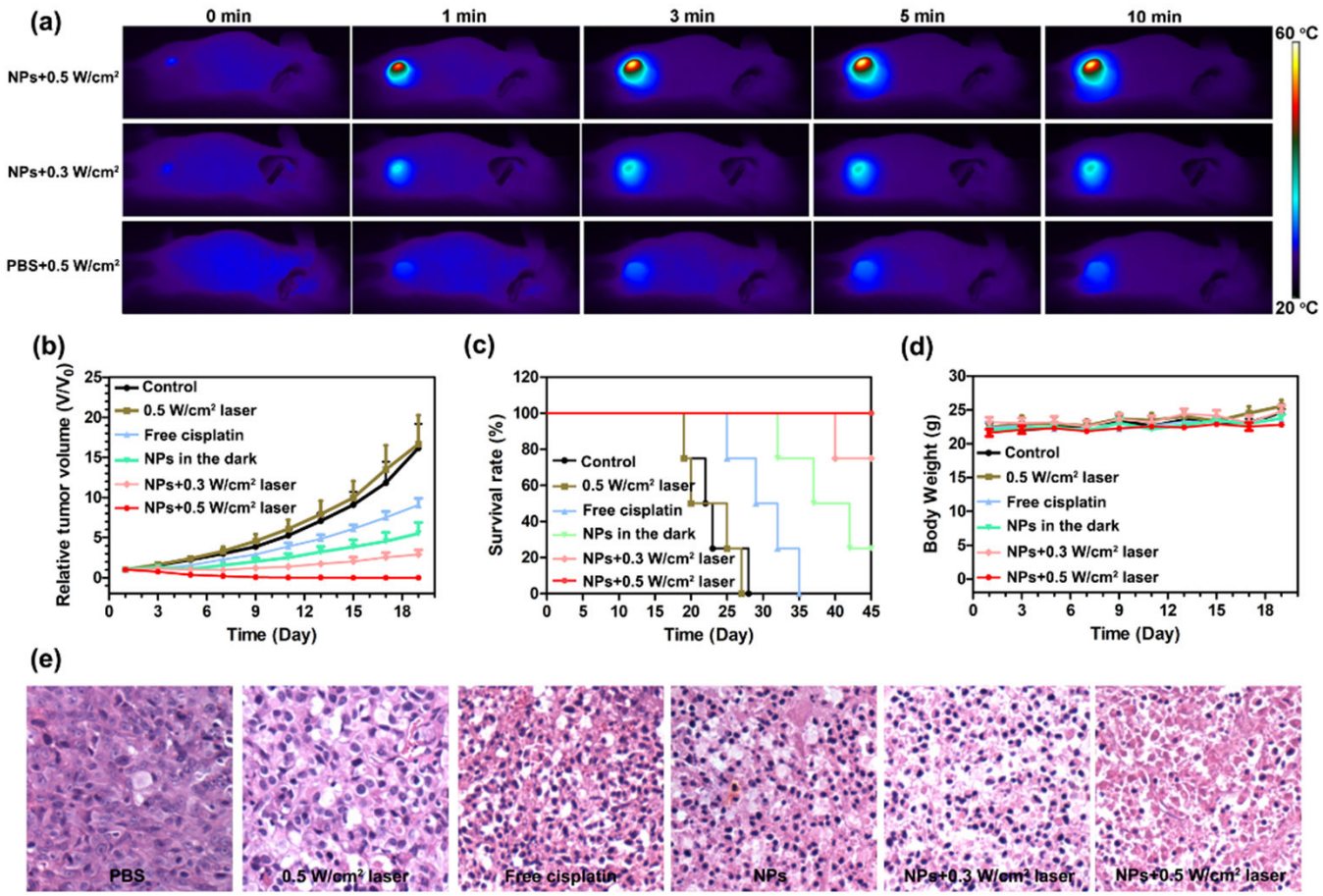

Fig. 4.

(a) *In vivo* infrared thermal images of U87MG tumour bearing mice with 671 nm laser irradiation after 24 h post-injection of GPDPA NPs or PBS by tail vein. The tumour section temperature rose from 28 °C to 48 °C within 5 min under GPDPA NPs administration and 0.5 W/cm^2 laser irradiation, whereas the tumour temperature only increased from 28 °C to 36 °C after PBS injection and the same intensity of laser power, indicating the excellent photothermal conversion performance and high tumour accumulation of GPDPA NPs. The relative tumour volume curves (b), survival curve (c) and the body weight of the mice under various treatments (d). The GPDPA NPs with 0.5 W/cm^2 laser irradiation led to complete tumour eradication and the GPDPA NPs with 0.3 W/cm^2 laser irradiation also inhibited the tumour growth significantly and improve the mice survival time. (e) The H&E-stained images of tumour sections acquired 48 h after various treatments. Tumour cell necrosis and apoptosis were found from GPDPA NPs with laser irradiation groups. Error bars (b, c and d), s.d. (n=4 replicates).

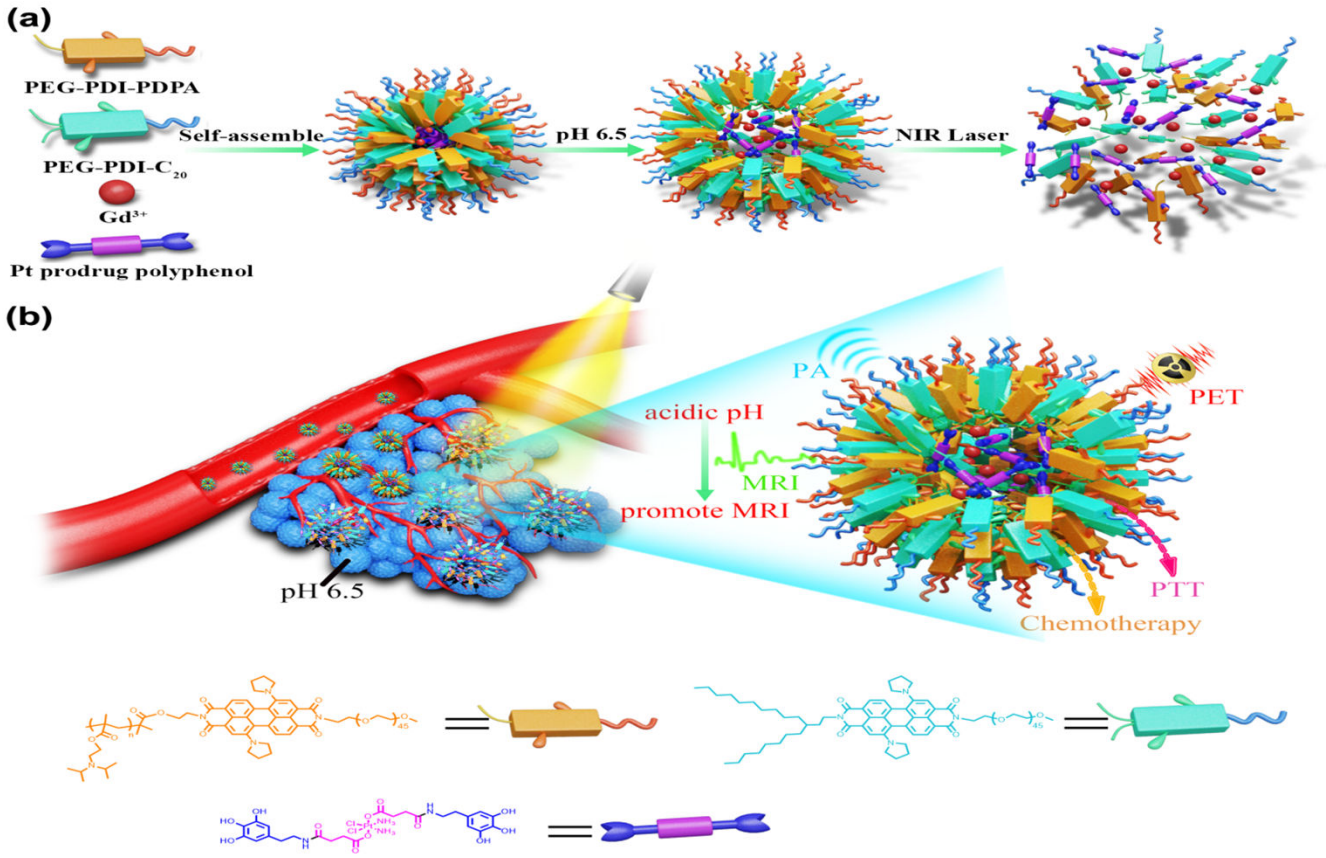

Scheme 1.

Schematic illustration of the formulation and cancer theranostics mechanism of the nanoparticles. (a) The self-assembly process of GPDPA NPs with mild acidic pH/NIR light-sensitive property. (b) The GPDPA NPs could accumulate in the tumour by EPR effect. The size of the GPDPA NPs grew by swelling and MR imaging signal was promoted in the acidic tumour microenvironment. The in vivo drug release and PA/MR/PET multimodal imaging guided chemo-photothermal combination therapy were achieved with NIR irradiation.

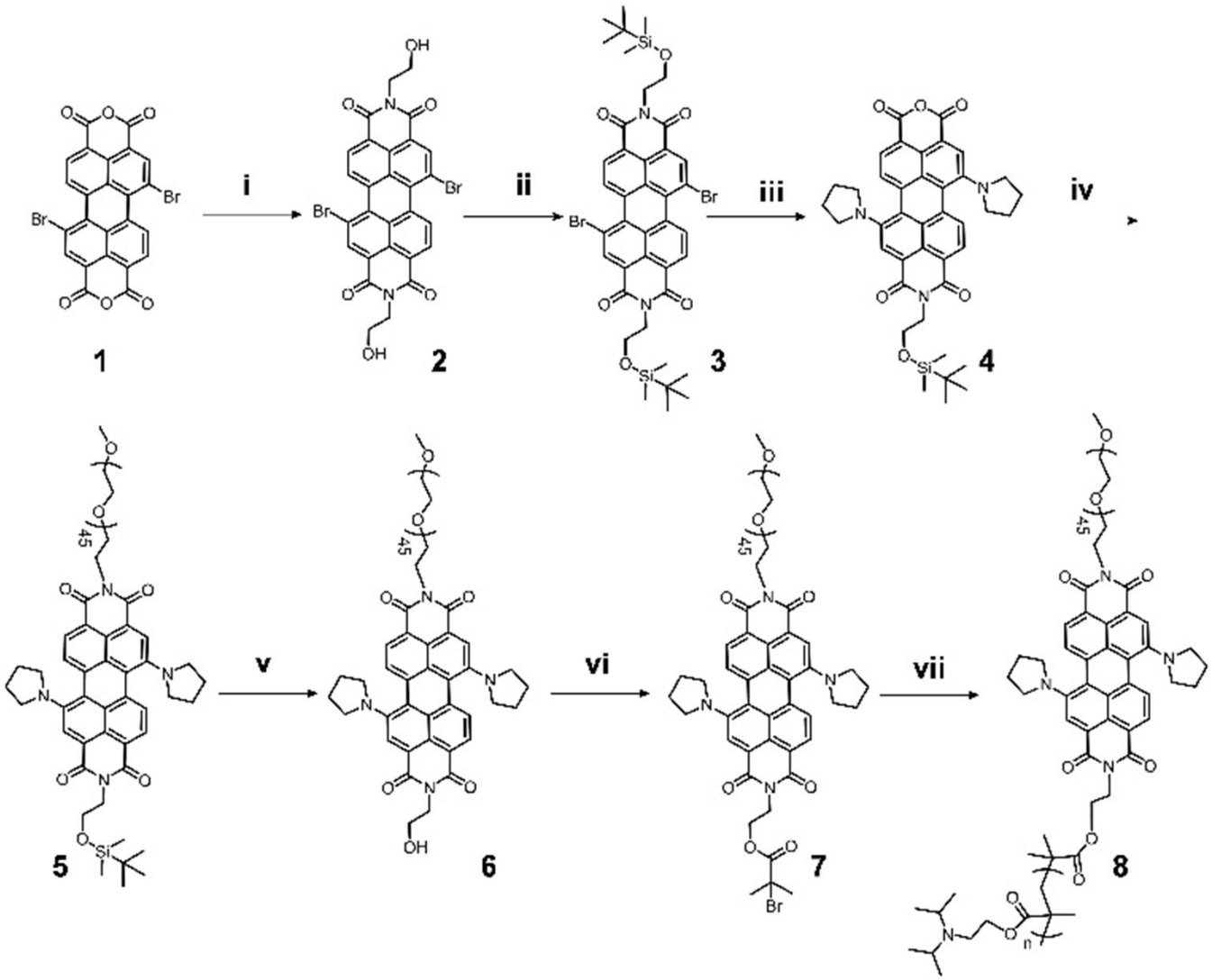

Scheme 2.

Design and synthesis of the PDI based pH sensitive polymer PEG-PDI-PDPA. Reaction conditions: (i) Ethanolamine, anhydrous N,N-dimethylformamide (DMF), 80 °C, 24 h. (ii) *tert*-Butyldimethylsilyl chloride, THF, room temperature. (iii) NaOH, *tert*-Butyl alcohol, 80 °C, 2h. (iv) mPEG2000-NH_2, imidazole, 120 °C, 1h. (v) TBAF, THF, room temperature. (vi) α-Bromoisobutyryl bromide, TEA, THF, room temperature. (vii) 2-(Diisopropylamino)ethyl methacrylate, CuBr, PMDETA, DMF, 80 °C.